Available online at www.sciencedirect.com
ScienceDirect
Planetary and Space Science 56 (2008) 1517–1523
Planetary and Space Science
www.elsevier.com/locate/pss

# Dry separation of respirable lunar dust: Providing samples for the lunar airborne dust toxicity advisory group

Yang Liu*, Darren W. Schnare, Benjamin C. Eimer, Lawrence A. Taylor

*Department of Earth and Planetary Sciences, Planetary Geosciences Institute, University of Tennessee, Knoxville, TN 37996, USA*

Received 28 May 2008; received in revised form 19 July 2008; accepted 5 August 2008
Available online 12 August 2008

**Abstract**

In order to study the toxicity of lunar dust, the respirable size fraction of lunar soil needed to be separated with an apparatus that possesses the following capabilities: no use of liquid; fully recoverable sample; and use of only small sample quantities ($<1$ gm). We report the design of a simple apparatus that meets these requirements and implements an inertial-impaction mechanism established in aerosol science. Lunar soil was agitated at a frequency of 100 Hz using a vibration table with a containment chamber under a constant air flow. The air flow carried the lofted lunar dust particles past four impactors (four T-junction connectors), upon which a fraction of large particles were captured during the impaction. The fine particles in the air flow were then collected by an end-of-the line membrane filter. Detailed examination of particles on the filter showed that the majority (~80–90 wt%) are $<3$ μm (geometric diameter), suggesting a high level of effectiveness for the apparatus.


*Keywords:* Particle separation; Lunar; Respirable dust; Toxicity

## 1. Introduction

Before establishing a human outpost on the Moon, numerous problems associated with lunar dust must be addressed and mitigated (Gaier, 2005; Taylor et al., 2005). The deleterious nature of lunar dust was experienced during all Apollo missions. Lunar dust (brought in on dirty spacesuits and boots) contaminated the atmosphere in the lunar module and irritated the eyes, sinuses, and throats of the astronauts (e.g., Gaier, 2005; Taylor et al., 2005). In contrast to short exposure times during the Apollo missions, astronauts partaking in missions of extended presence on the Moon will be subjected to prolonged exposure if lunar dust contamination is not substantially mitigated. Therefore, the physiological effects of lunar dust on humans need to be known, and this topic is being actively studied by a mutiple-disciplinary group of scientists, the Lunar Airborne Dust Toxicity Analyses Group (LADTAG) (Jones et al., 2008; Khan-Mayberry, 2008; Lam et al., 2008).

Many epidemiological studies have found statistically significant links between ambient particulate-matter levels and human-health endpoints (mortality, pulmonary-function decrease, respiratory diseases, etc.) (see references in EPA 1996, 2004). Based on these studies, the US Environmental Protection Agency has regulated pollution standards for airborne particulate matters (PMs) with aerodynamic diameters of $\leqslant 10$ and $\leqslant 2.5$ μm (EPA 1996, 2004). Aerodynamic diameter ($D_a$) is the diameter of a unit-density sphere with the same settling velocity of the particle in question (e.g., Reist, 1993). OSHA defined the respirable dust fraction to be PMs with $D_a \leqslant 3.5$ μm. Obeying this strict definition, the respirable fraction of lunar dust is composed of $>80$ wt% glass (Taylor et al., 2001) with high abundances of nanophase metallic iron (np-$Fe^0$), which may be highly toxic to humans, as discussed below. For toxicity studies, it is important to obtain the respirable fraction without any modification to particle surface properties. Therefore, dry-separation techniques are required. However, existing fine-particle separators (e.g., virtual impactors, cyclones, cascade impactors) typically involve greased surfaces in order to limit contamination of larger particles and to collect the $<2.5$ μm PM

*Corresponding author. Tel.: +1 865 974 6024; fax: +1 865 974 2368.
*E-mail address:* yangl@utk.edu (Y. Liu).

0032-0633/$ - see front matter © 2008 Elsevier Ltd. All rights reserved.
doi:10.1016/j.pss.2008.08.003

(EPA, 1996). Because lunar samples are precious and of limited quantity, an apparatus that uses a small quantity of sample (<1 gm) and allows for almost total sample recovery would be ideal. In this study, we illustrate the design of an apparatus (Dry-Aerosol-Impactor Size-Separator, hereafter referred to as DAISS) capable of dry separation of a small amount (<1 gm) of bulk sample to <3 μm (geometric diameter).

Three lunar highland soils and one lunar dust simulant were subjected to the DAISS. Particle-size distribution (PSD) of the separated samples confirmed that the apparatus can efficiently separate the <3 μm fraction.

## 2. Properties of lunar dust

Lunar dust, the <20 μm size fraction of the soil on the Moon (using the definition adopted by LADTAG), constitutes ~20 wt% of the soil (Carrier, 2003; McKay et al., 1991). Lunar soil/dust contains nanophase metallic iron in agglutinitic glass and in vapor deposited rims on soil particles, which are formed through the process of "space weathering" (e.g., Pieters et al., 2000; Taylor et al., 2001; Hapke, 2001; Hapke et al., 1994). Unprotected, due to a lack of an effective atmosphere ($10^{-12}$ Torr), the surface of the Moon has been continuously bombarded by the full force of meteorites and micrometeorites for the last 4.5 Ga. These impacts most commonly just pulverize rocks and minerals, but some have pulverize rocks and minerals, but some have sufficient energy to actually melt the lunar soil. At the same time, the hypervelocity (30,000 to >100,000 km/h) of the impacting micrometeorites (<1 mm) can supply sufficient kinetic energy to not only melt portions of the soil, but to vaporize certain elements/oxides from the melt. This vapor is re-deposited as silica-rich glass coatings or "patinas" on the surfaces of soil particles, and this glass contains myriads of dispersed nanophase metallic iron (Keller and McKay 1993, 1997; Wentworth et al., 1999). The size of these metallic iron grains (np-$Fe^0$) ranges from ~3 to 30 nm (Keller and Clemett, 1997; Keller and McKay, 1993). These np-$Fe^0$ grains, acting as pairs and triplets, impart a ferromagnetic susceptibility to the lunar soil (Taylor et al., 2005). Continuous bombardments by meteorites and micrometeorites further break and melt soil particles. The impact-generated melt quenches and acts as a cement to aggregate rock and mineral particles to form agglutinates (McKay et al., 1991). Agglutinitic glasses (quenched melts) thus contain abundant and slightly coarser-iron globules (e.g., mean size of ~140 nm; James et al., 2002, 2003).

## 3. Toxicity of lunar dust

The respirable portions of lunar dust may be highly toxic, especially given this abundance of np-$Fe^0$ in the impact glass. As an analogy, the <3 μm fraction of terrestrial dust particles is known to be correlated with adverse cardiovascular diseases (Delfino et al., 2005; EPA, 1996; and references therein). Safety concerns, with respect to nano-particles, have become the focus of attention in recent years with the advance of nanotechnology (e.g., Nel et al., 2006; Fubini and Fenoglio, 2008). For lunar dust, significant portions of the particles are <0.1 μm (geometric diameter), as determined by the PSD study of Park et al. (2006, 2008). These <100 nm particles are, on average, slightly elongated with vaguely complex shapes (Liu et al., 2006–2008). The abundance of np-$Fe^0$-bearing, impact-generated glass increases with decreasing grain size fractions of lunar soil/dust; such glass constitutes ~80% of the <1 μm fraction of a mature lunar soil (Basu et al., 2002; Taylor et al., 2001, 2003). Therefore, fine (<3 μm) to ultrafine (<0.1 μm) particles of lunar dust consist almost entirely of impact glass, much of which contains np-$Fe^0$. This highly meta-stable impact glass may be easily dissolved in bodily fluids, thereby releasing the np-$Fe^0$ grains, which are very reactive, owing to their redox potential and relative large surface area per unit mass (Liu et al., 2008). It is obvious that this fine fraction of the lunar soil, the dust, must be studied for potential toxicity to humans. Such studies are currently being performed by the NASA LADTAG centered at Johnson Space Center and Ames Research Center (Khan-Mayberry, 2008; Lam et al., 2008; Prisk and Darquenne, 2008; Tranfield et al., 2008).

## 4. Methodology

### 4.1. Sample selection

Test runs were conducted on 5 g of lunar soil simulant JSC-1Avf, which is a specially prepared dust fraction (<20 μm) from a new batch (JSC-1A) of lunar soil simulant JSC-1. These simulants were made from the same volcanic welded-tuff (McKay et al., 1994) to approximate only the physical/geotechnical properties of lunar soil (Klosky et al., 1996). The mineral constituents and compositions of JSC-1A and JSC-1 are atypical for most lunar soils (Hill et al., 2007). The following Apollo 16 lunar highland soils were used in this study: 61501, $I_s$/FeO = 53, submature; 62241, $I_s$/FeO = 100, mature; and 64801 $I_s$/FeO = 71, mature. The ratio of $I_s$/FeO is the maturity index, defined by Morris (1978), reflecting soil maturity and the relative abundance of nanophase Fe in the impact glass. All lunar soils were previously dry sieved to <1 mm at Johnson Space Center. About 5 g of soils 61501 and 62241, and 1 g of soil 64801 were used for our separation experiments. After separation, samples were carefully recovered and weighed. The recovery was 97–98 wt%.

### 4.2. Instrumentation

The DAISS was developed by employing the inertial-impaction mechanism of particle kinetics. Upon impacting a stationary object, particles in a flowing air stream will be fractionated according to their size. Larger particles are less adaptive to changes in flow conditions (direction and

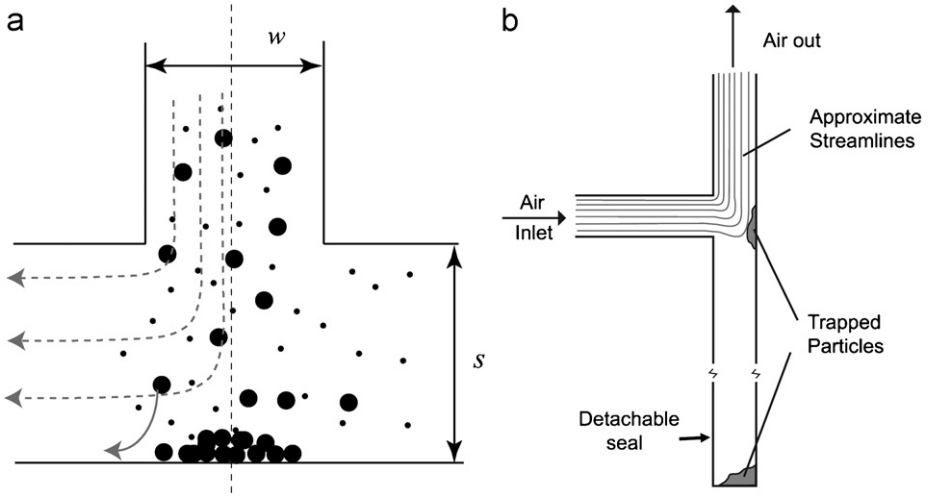


Fig. 1. Schematic diagram of the impactor. Lines illustrate path of air flow through the impactor. (a) Illustration of particles flowing through a flat-plate impactor. $w$ is the nozzle diameter, and $s$ is the nozzle-to-plate distance. (b) Schematic streamlines in the plastic "T"-connector used as impactor. One end of the "T"-connector is sealed off so that air mainly flows toward one direction. As particles build up on the wall of the impactor, they flake off into the sealed end so that they are out of the way of the air flow.

velocity), some of which will be captured by the stationary plate (Fig. 1a). Inertial impaction is not efficient for smaller particles (especially $<0.3\,\mu m$), and thus, the small particles are more likely to be entrained in the flowing stream (Fig. 1a). The fractionation of large particles depends on factors such as Reynolds number ($Re$), nozzle shape (diameter, $w$), the nozzle-to-plate distance ($s$), and flow direction (Reist, 1993). Our simple design implemented a series of "T"-shaped connectors with a round cross-section (ID = 5.8 mm) as impactor plates. One end of the connector was closed with a detachable seal (Fig. 1b), and thus, the air flow was forced into a 90° turn. The schematic flow streamlines are shown in Fig. 1b. Particles captured by the impactor were collected in the seal and were out of the air flow path. The "T"-shape of the connector yields a $w/s$ ratio of 1.

The apparatus consists of a compressed-air source, rotameter, sample chamber, vibration table, four impactors, a membrane filter, and flexible tubing that connects the different parts together (Fig. 2). The sample chamber consists of a silica-glass tube, a metal top plate with air inlet and outlet, and an O-ring seal (inset in Fig. 2). The first impactor and the air outlet of the sample chamber have different sizes. To connect them and to ensure efficient fractionation of particles, a small tube of the same size as the air outlet is inserted into the first impactor. Then, this small tube is connected to the outlet of the sample chamber with a flexible tubing of 3.5 mm inner diameter. Ultra-smooth Tygon tubings with an inner diameter of 7 mm are used for all other parts. All tubes are short in order to minimize particle capture by Brownian diffusion, a process whereby particles in the range of 0.01–0.1 μm are easily deflected by air molecules to random directions. This random movement makes these particles more prone to be captured by the walls of the

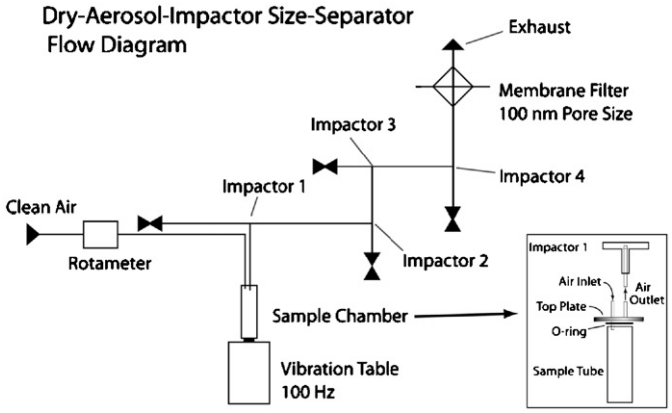


Fig. 2. Flow diagram of the aerosol trap. The inset shows the details of the sample chamber.

tubing. A membrane filter (purchased from Milipor$^{TM}$) of 4.7 cm diameter is used to collect particles of interests (i.e., $<3\,\mu m$) at the end of the separation line. The filter is made of hydrophobic polyvinylidene difluoride (PVDF) fibers with 0.1 μm pore size for liquids. The filter is sealed using an O-ring in a holder.

About 1–5 g of sample was sealed in the sample chamber, which was then affixed to the top of the vibration table. Clean compressed air was directed into the sample tube at a flow rate of $\sim 1.6\times10^{-4}\,m^3/s$. Given the diameter of T-shaped connectors and tubes, this flow rate transfers to an air-flow velocity of ~6 m/s. By agitating the sample at a frequency of 100 Hz, particles can be levitated and lofted by the convecting air in the chamber, and then carried to the impactors. During this agitation process, the first particle fractionation occurs—i.e., only particles of a certain size could be levitated by the air. At the first impactor, flow velocity decreased due to an increase in the

cross-sectional area. Consequently, particle fractionation occurs through the decrease in flow velocity, as well as the flow direction. Most large particles were captured at the first impactor. For each of the following impactors, the fractionation solely occured by the change of the flow direction, which removed a portion of the remaining large particles. After intercepting the filter, the air flow exited the system. At the conditions specified above, the collection rate on the membrane filter is ~10–20 mg/h for 5 g of starting sample.

### 4.3. Particle-size measurements

The PSDs for powders collected on the filter were determined using the imaging method of Park et al. (2008) and is summarized below.

To disperse particles, a surfactant solution (poly N-vinylpyrrolidone in isopropanol) was added to samples at a ratio of 1 mg sample per 1 ml of solution. This mixture was lightly sonicated for 10–15 min to separate attached particles. Park et al. (2006, 2008) determined that this was sufficient to detach smaller particles from the surfaces of larger ones without measurably changing the grain size of larger particles. Around 2.5 μl of the mixture was then taken with a micropipette, dropped on a silicon wafer placed above a strong Nd-magnet. The presence of the magnet affected the nanophase metallic iron in the dominant impact glass and kept particles from clumping together during evaporation of the dispersive solution. Having the particles separate from one another is crucial to studies of this nature, as it would change the measured particle sizes. If clumping does occur, particles that overlap or touch have to be "separated" during digital processing of the images.

Digital images of these samples were taken with a JEOL LSM-6060LV scanning electon microscope (SEM) at two different magnifications (1000X and 5000X). The spatial resolution is 0.1 μm/pixel at 1000X, and 0.02 μm/pixel at 5000X. Pictures were taken along three orthogonal radii of this circular spread. The contrast and brightness of particles were optimized for the ease of data processing. Images at 1000X were taken starting at the center, and then every 0.5 mm. Images at 5000X are required to adequately make determinations on the fine particles. Thus, for each 1000X image, 25 images were taken at 5000X, the amount required to cover the same area as the 1000X images. Just as higher magnification images are better for fine particles, so images at the lower magnification are better for determinations on large particles. We then compiled the data-sets to obtain the best results. For each radius, particles measured in the 1000X images were combined with those from 5000X images and then projected to the whole circular loop. Results from the three orthogonal radii were averaged to obtain the final distribution.

The software ImageJ (http://rsb.info.nih.gov/ij/) was used to determine the area and perimeter of every particle within each image. Particles were measured through image thresh-holding. Touching particles were separated manually by 1 pixel. Particles cutoff by the edge of the image were ignored. Because the $z$-direction in SEM images cannot be calibrated, photos of the particles were considered as 2D projections. The size of the particle was represented by the diameter of a circle that is equivalent to the measured area ($D_{pa}$).

## 5. Results and discussion

### 5.1. Validation of image-analysis method

The PSDs on the basis of the 2D diameters by the SEM method need to be compared to those for 3D diameters by other techniques, such as light diffraction methods, which directly determine the 3D sphere-equivalent diameter ($D_v$). A correction factor is needed to compare these two diameters. To determine this factor, we compare the PSDs of the pre-separation lunar dust simulant JSC-1Avf determined with our image-analysis method with those from light-diffraction methods, such as a Coulter-type particle size analyzer using visible light and a Microtrack particle size analyzer using laser sources (Fig. 3).

Corrections from 2D projections to 3D spheres have been suggested by Davies (1979) and Thornburg et al. (2006). The projected 2D diameter ($D_{pa}$) can be transformed to a volumetric diameter ($D_v$), the diameter of a sphere with an equivalent volume, by applying a volume shape factor, $k$, so that

$$D_v = D_{pa} * k$$

The measured $k$ (expressed as $\phi_v/d_p$ in Table 2, Davies, 1979) ranges from 0.68 for talc and limestone, to 0.71 for furnace slag, and to 0.79 for sand. This transfers to a volume shape factor of 0.76–0.84. Fig. 3 shows the

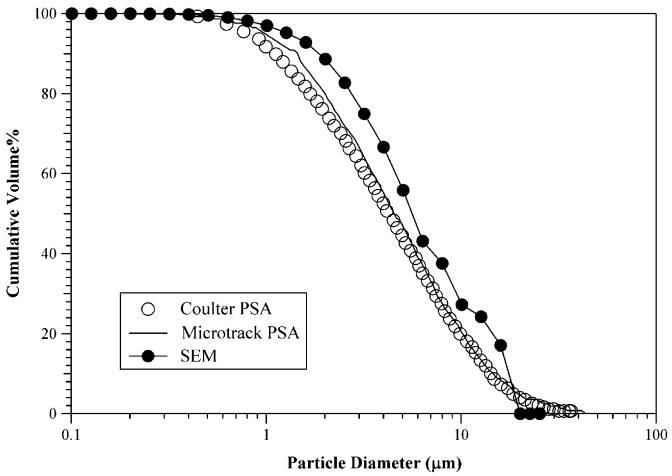


Fig. 3. Particle size distributions (PSD) of JSC-1Avf determined with different methods. The 3D sphere-equivalent diameters ($D_v$) were plotted for light diffraction methods, Coulter-type Particle Size Analyzer (PSA) and Microtrack laser PSA (adapted from David McKay). The 2D projected area diameter ($D_{pa}$) is plotted for SEM method.

cumulative plots for JSC-1Avf from these three methods. The shapes of distribution curves among three different methods are significantly similar. The cumulative plot from SEM method is displaced to larger particle sizes by a factor of 1.25, corresponding to $k = 0.8$. Liu et al. (2007, 2008) showed that the particle morphologies are similar between JSC-1Avf and the $<45\,\mu m$ fraction of lunar soils. Therefore, this correction factor is applicable to lunar samples.

To compare the equivalent sphere diameter ($D_v$) with the aerodynamic diameter ($D_a$), an additional conversion is necessary. Because $D_a$ is defined as the diameter of a unit-density sphere with the same settling velocity as the particle of interest, the conversion between $D_a$ and $D_v$ follows:

$$D_a = D_v[\rho_p C_{c,D_v}]/(\chi\rho_0 C_{c,D_a})]^{0.5},$$

where $\rho_p$ is the density of the particle, $\rho_0$ is the unit density ($1000\,kg/m^3$), $\chi$ is the dynamic-shape factor, $C_{c,\,D_v}$ and $C_{c,\,D_a}$ are the Cunningham slip-correction factors for $D_v$ and $D_a$. The dynamic-shape factor ($\chi$) corrects for the effect of the irregular shape of the actual particle on the settling velocity. Davies (1979, Table 18) determined $\chi$ for a range of materials including mineral dust. We select the factor for sand (1.57) in the following discussion.

When particles are smaller than the distance between molecules of a medium, the resisting force offered to the particle is smaller than predicted from the perfect Stokes' law. Thus, the Cunningham slip-correction factor is used to correct for this effect. For particles larger than the free mean path (distance between molecules) of dry air ($0.069\,\mu m$) at $20\,^{\circ}C$, we can ignore $C_c$ and approximate $D_a$ by

$$D_a \approx D_v[\rho_p/\rho_0\chi]^{0.5}$$

If using $\chi$ of 1.57 and a density of $2600\,kg/m^3$, $D_a \approx 1.3 D_v$.

### 5.2. Effectiveness of the apparatus

The effectiveness of the DAISS apparatus is shown by PSDs and accumulative volume plots of all four samples (Fig. 4). The PSDs of all separated samples show a mode at 0.4–0.6 μm, whereas 80–90 wt% of separated samples are $<3\,\mu m$ ($D_v$). If using $\chi$ of 1.57 and a density of $2600\,kg/m^3$, 80–90 wt% of all samples are less than an aerodynamic diameter of ~4 μm, and ~50 wt% of all samples are less than ~3 μm (aerodynamic diameter). These results show that the performance of the DAISS apparatus is consistent for different samples with different base characteristics. The most important result is that all lunar soils tested, as well as the lunar dust simulant, JSC-1Avf, can be separated to the targeted size of $<3\,\mu m$.

### 5.3. Comparison with impaction principle for a flat-plate impactor

The principles of impaction for a flat-plate impactor have been well modeled. The collection efficiency of such impactors is a function of Stokes number, Stk, and

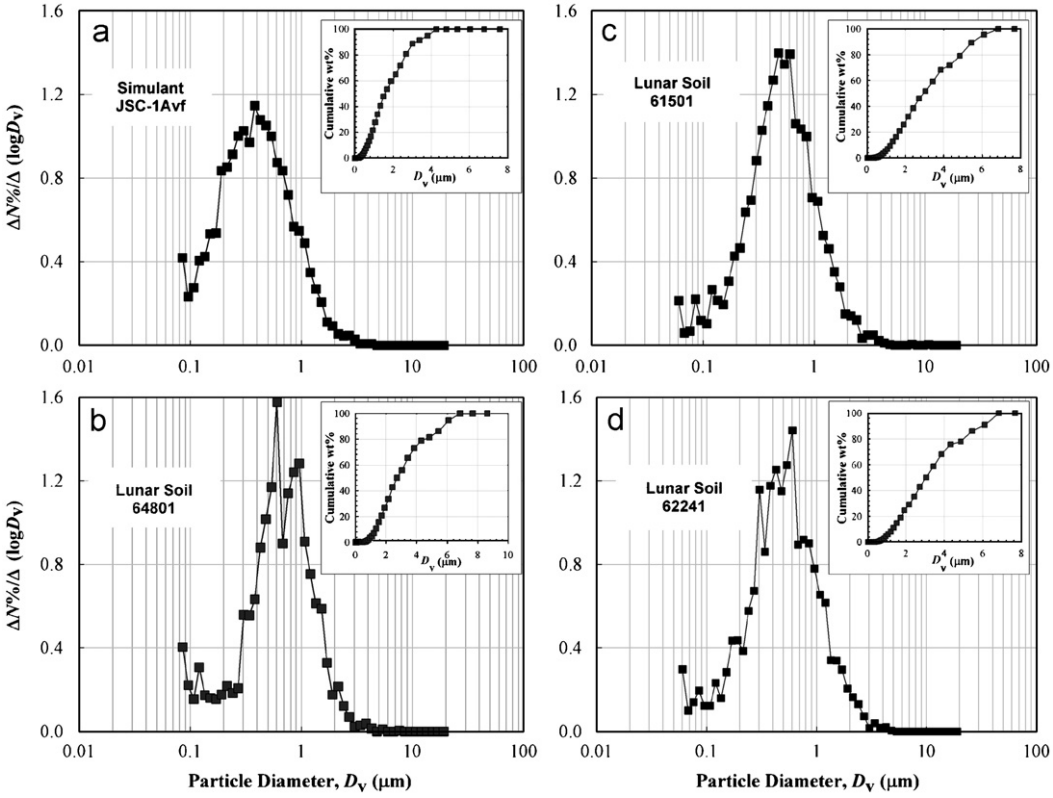


Fig. 4. Particle size distribution (PSD) of separated samples collected on the filter.

Reynolds number, *Re* (Marple and Liu, 1974; Marple and Willeke, 1976):

$$\mathrm{Stk} = (\rho_p C_c D_p^2 U)/(9\mu_a W)$$

$$Re = (\rho_a U W)/\mu_a$$

where $\rho_p$ and $\rho_a$ are particle and air density; $C_c$ is the Cunningham slip-correction factor; $U$ is the velocity of air stream; $\mu_a$ is the dynamic viscosity of air; $D_p$ is particle diameter (or $D_v$); and $W$ is the diameter of the air inlet. The removal of particles at the impactor is commonly expressed as an efficiency curve plotted with $(\mathrm{Stk})^{0.5}$ (Reist, 1993). The collection characteristic of an impactor is often expressed as $\mathrm{Stk}_{50}$, the Stk at 50% efficiency. For particles with $\mathrm{Stk} < \mathrm{Stk}_{50}$, the removal efficiency is small, and they tend to stay in the flow. The collective efficiency of a flat-plate impactor for different impactor shapes, Stk, *Re*, and particle density were examined experimentally and theoretically (Huang and Tai, 2002; Marple and Liu, 1974; Marple and Willeke, 1976; Rader and Marple, 1985). From these studies, the $\mathrm{Stk}_{50}$ for a round nozzle converges to 0.21–0.25 for $\mathrm{Re} \geqslant 3000$ and particle density $> 1000\,\mathrm{kg/m^3}$.

There is no theoretical modeling for the "T"-shaped connector with a curved inner wall and limited size in one direction. However, we use the above equations as a first-order approximation of the efficiency in removing particles larger than 3–5 μm. For DAISS, $W$ is 5.8 mm, the air-flow velocity is 6 m/s, and air viscosity and air density at 15 °C and sea level are $1.8 \times 10^{-5}$ Pa s and $1.225\,\mathrm{kg/m^3}$. We assume a uniform density of $2600\,\mathrm{kg/m^3}$ for the $<4\,\mu\mathrm{m}$ fraction of lunar particles, because they are mainly composed of np-$Fe^0$ bearing glass. From these conditions, the *Re* for the DAISS is 2368. $C_c$ increases significantly with decreasing particle size, especially for particles $<1\,\mu\mathrm{m}$. For particles larger than 3 μm, $C_c$ only increases slightly from 1.02 for 10 μm particles to 1.06 for 3 μm particles (Reist, 1993). Because we are concerned about the efficiency in removing particles $>3\,\mu\mathrm{m}$, $C_c$ is 1.02–1.06, which corresponds to particle diameters range from 3.3 to 3.7 μm for $\mathrm{Stk}_{50}$ of 0.21–0.25. Given the approximated nature of the above calculations, it is interesting that particles collected on the filter are mostly $<5\,\mu\mathrm{m}$, very close to the predicted value. The slightly larger size could be caused by turbulent air stream from the curved inner wall and/or random particle deflections. Given these complications, the similar results for all samples, with 80–90 vol% of particles $<5\,\mu\mathrm{m}$, suggest the consistent reproducibility of the DAISS.

## 6. Summary

In order to process small quantities of lunar dust samples in a dry mode and ensure maximum recovery of the sample, an apparatus utilizing aerosol impaction on stationary plates was developed to separate lunar dust from bulk lunar soil. This apparatus can efficiently separate the $<3\,\mu\mathrm{m}$ fraction of dust from different lunar soils, as well as the lunar soil simulant JSC-1Avf. Samples produced by this method will be quite useful in studies on the toxicological and physiological effects of lunar dust inhalation by the LADTAG scientists.

## Acknowledgements

The thorough, constructive reviews of Sarah Noble and Abhijit Basu significantly improved the initial manuscript. This research has been supported by the NASA grant from the Lunar Airborne Dust Toxicity Advisory Group (LADTAG), for which we are grateful. Helpful discussions with the LADTAG members added significantly to this study. Additional funding was provided by the Planetary Geosciences Institute at the University of Tennessee.

## References

Basu, A., Wentworth, S.J., McKay, D.S., 2002. Heterogeneous agglutinitic glass and the fusion of the finest faction ($F^3$) model. Meteorit. Planet. Sci. 37, 1835–1842.

Carrier III, W.D., 2003. Particle size distribution of lunar soil. J. Geotech. Geoenviron. Eng. 129, 956–959 ASCE.

Davies, C.N., 1979. Particle-fluid interaction. J. Aerosol Sci. 10, 477–513.

Delfino, R.J., Sioutas, C., Malik, S., 2005. Potential role of ultrafine particles in associations between airborne particle mass and cardiovascular health. Environ. Health Perspect. 113, 934–946.

EPA, 1996. US EPA. Air Quality Criteria for Particulate Matter, Volumes I–III. US Environmental Protection Agency, Washington, DC, EPA/600/P-95/001aF to -001cF.

EPA, 2004. US EPA. Air Quality Criteria for Particulate Matter, Volumes I–III. US Environmental Protection Agency, Washington, DC. EPA/600/P-99/002aF to /002bF.

Fubini, B., Fenoglio, I., 2008. Toxic potential of mineral dusts. Elements 3, 407–414.

Gaier, J. R., 2005. The effects of lunar dust on EVA systems during the Apollo missions, NASA, GRC. NASA/TM-2005-213610.

Hapke, B., 2001. Space weathering from Mercury to the asteroid belt. J. Geophys. Res.—Planets 106, 10039–10073.

Hapke, B., Cassidy, W., Wells, E., 1994. Vapor deposits in the lunar regolith. Science 264, 1779.

Hill, E., Mellin, M.J., Deane, B., Liu, Y., Taylor, L.A., 2007. Apollo sample 70051 and low- and high-Ti lunar soil simulants MLS-1A and JSC-1A: implications for future lunar exploration. J. Geophys. Res. 112, E02006.

Huang, C-H., Tai, C-J., 2002. Influence of impaction plate diameter and particle density on the collection efficiency of round-nozzle inertial impactors. Aerosol Sci. Technol. 36, 714–720.

James, C. L., Letsinger, S. L., Basu, A., Wentworth, S. J., McKay, D. S., 2002. Size distribution of Fe0 globules in lunar agglutinitic glass. LPS XXXIII, Abstract # 1827.

James, C. L., Letsinger, S. L., Basu, A., Wentworth, S. J., McKay, D. S., 2003. Nanophase iron globules in lunar soil. LPS XXXIV, Abstract # 1992.

Jones, L., Jacques, S., Rask, J.C., Tranfield, E., Taylor, L., Kerschmann, R., Loftus, D.J., 2008. Lunar dust biological effects, NLSI Lunar Science Conference, Abstract # 2100.

Keller, L.P., Clemett, S.J., 1997. Formation of nanophase iron in the lunar regolith. Lunar Planet. Sci. XXXVII (CD-ROM), Abstract # 2097, Lunar and Planetary Institute, Houston.

Keller, L.P., McKay, D.S., 1993. Discovery of vapor deposits in the lunar regolith. Science 261, 1305–1307.

Keller, L.P., McKay, D.S., 1997. The nature and origin of rims on lunar soil grains. Geochim. Cosmochim. Acta 61, 2331–2341.

Khan-Mayberry, N.N., 2008. Living on the lunar surface: determining the health effects of exposure to respirable lunar dusts. NLSI Lunar Science Conference, Abstract # 2081.

Klosky, J.L., Sture, S., Ko, H.Y., Barnes, F., 1996. Mechanical properties of JSC-1 lunar regolith simulant. Space V, ASCE, 680–688.

Lam, C.-W., James, J.T., Khan-Mayberry, N., Hammond, D., Hunter, R., McCluskey, R., Taylor, L., Chen, B.T., Erdely, P.C., Castranova, V., 2008. Pulmonary toxicity studies of lunar dust in rodents, NLSI Lunar Science Conference, Abstract # 2136.

Liu, Y., Park, J., Hill, E., Kihm, K., Taylor, L.A., 2006. Morphology and physical characteristics of Apollo 17 dust particles. Earth & Space 2006, American Society for Civil Engineers Proceedings, CD-ROM.

Liu, Y., Park, J.S., Schnare, D.W., Kihm, K.D., Hill, E., Taylor, L.A., 2008. Characterization of lunar dust for toxicological studies: part 2- texture and shape characteristics. J. Aerosp. Eng. 21 (4), 272–279.

Liu, Y., Schnare, D., Park, J.S., Hill, E., Eimer, B., Taylor, L.A., 2007. Shape analyses of lunar dust particles for astronaut toxicological studies. LPSC XXXVIII, Abstract #1383.

Marple, V.A., Liu, B.Y.H., 1974. Characteristics of laminar jet impactors. Environ. Sci. Technol. 8, 648–654.

Marple, V.A., Willeke, K., 1976. Impactor design. Atmos. Environ. 10, 891–896.

McKay, D.S., Heiken, G., Basu, A., Blanford, G., Simon, S., Reedy, R., French, B.M., Papike, J., 1991. The lunar regolith. In: Heiken, G., Vaniman, D., French, B. (Eds.), Lunar Sourcebook. Cambridge University Press, New York, pp. 286–356.

McKay, D.S., Carter, J.L., Boles, W.W., Allen, C.C., Allton, J.H., 1994. JSC-1: a new lunar soil simulant. Space IV, ASCE, 857–866.

Morris, R.V., 1978. The surface exposure (mature) of lunar soils: some concepts and Is/FeO compilation. Proc. Lunar Planet. Sci. Conf. 9th, 2287–2297.

Nel, A., Xia, T., Madler, L., Li, N., 2006. Toxic potential of materials at the nanolevel. Science 311, 622–627.

Park, J., Liu, Y., Kihm, K., Hill, E., Taylor, L.A., 2006. Submicron particle size distribution of Apollo 11 lunar dust. Earth & Space 2006, American Society for Civil Engineers Proceedings, CD-ROM.

Park, J.S., Liu, Y., Kihm, K.D., Taylor, L.A., 2008. Characterization of lunar dust for toxicological studies: part 1- particle size distribution. J. Aerosp. Eng. 21 (4), 266–271.

Pieters, C.M., Taylor, L.A., Noble, S.K., Keller, L.P., Hapke, B., Morris, R.V., Allen, C.C., McKay, D.S., Wentworth, S., 2000. Space weathering on airless bodies: resolving a mystery with lunar samples. Meteorit. Planet. Sci. 35, 1101–1107.

Prisk, G.K., Darquenne, C., 2008. Deposition and clearance of dust particles in the human lung in lunar gravity, NLSI Lunar Science Conference, Abstract # 2076.

Rader, D.J., Marple, V.A., 1985. Effect of ultra-Stokesian drag and particle interception on impaction characteristics. Aerosol Sci. Technol. 4, 141–156.

Reist, P.C., 1993. Aerosol Science and Technology. McGraw-Hill, Inc, p. 379.

Taylor, L.A., Pieters, C.M., Keller, L.P., Morris, R.V., McKay, D.S., 2001. Lunar mare soils: space weathering and the major effects of surface-correlated nanophase Fe. J. Geophys. Res. 106, 27985–27999.

Taylor L. A., Pieters C.M., Patchen A., Taylor D.-H., Morris R.V., Keller L.P., McKay D.S., 2003. Mineralogical characterization of lunar highland soils. LPS XXXIV, Abstract # 1774.

Taylor, L. A., Schmitt, H.H., Carrier, W.D., Nakagawa, M., 2005. The lunar dust problem: from liability to asset. 1st Space Exploration Conference AIAA, CD-ROM, AIAA2005-2150 AIAA 〈http://hefd.jsc.nasa.gov/toxladtag.htm〉.

Thornburg, J., Rodes, C., Lamvik, M., Willis, R., Rosati, J., 2006. Image analysis method (IAM) for measurement of particle size distribution and mass availability on carpet fibers. Aerosol Sci. Technol. 40, 274–281.

Tranfield, E., Rask, J.C., Wallace, W.T., Taylor, L., Kerschmann, R., James, J.T., Khan-Mayberry, N., Loftus, D. J., the LADTAG Research Working Group, 2008. Lunar airborne dust toxicity advisory group (LADTAG), Research Working Group (RWG). NLSI Lunar Science Conference, Abstract # 2076.

Wentworth, S.J., Keller, L.P., McKay, D.S., Morris, R.V., 1999. Space weathering on the Moon: patina on Apollo 17 samples 75075 and 76015. Meteorit. Planet. Sci. 34, 593–603.